Diatom flux reflects water-mass conditions on the southern Northwind Abyssal Plain, Arctic Ocean

J. Onodera[*1], E. Watanabe[1], N. Harada[1], M. C. Honda[2]

[1]Research and Development Center for Global Change, Japan Agency for Marine-Earth Science and Technology, Natsushima-cho 2-15, Yokosuka, 237-0061, Japan

[2]Department of Environmental Geochemical Cycle Research, Japan Agency for Marine-Earth Science and Technology, Natsushima-cho 2-15, Yokosuka, 237-0061, Japan

*Corresponding author: onoderaj@jamstec.go.jp

ABSTRACT:

We studied time-series fluxes of diatom particles from 4 October 2010 to 18 September 2012 using bottom-tethered moorings with two sediment traps deployed at 180 m and 1300 m depths at Station NAP (75°N, 162°W; 1975-m water depth) in the western Arctic Ocean. This paper discusses on the relationship of time-series diatom fluxes with satellite-based sea ice motion and simulated hydrographic variations. We observed clear maxima of the diatom valve flux in November–December of both 2010 and 2011, and in August 2011. Diatoms in samples were categorized into 98 taxa. The diatom flux maxima were characterized by many resting spores in November–December and by the sea ice-associated diatom *Fossula arctica* in August 2011. These assemblages along with abundant clay minerals in the samples suggest a significant influence of shelf-origin materials transported by mesoscale eddies, which developed along the Chukchi Sea shelf break. In contrast, the fluxes of total mass and diatoms were reduced in summer 2012. We hypothesize that this suppression reflects the influx of oligotrophic water originating from the central Canada Basin. A physical oceanographic model demonstrated that oligotrophic surface water from the Beaufort Gyre was supplied to Station NAP from December 2011 to early half of 2012.

KEY WORDS: diatom, phytoplankton, sinking particle flux, sediment trap, Northwind Abyssal Plain, Arctic Ocean

1. Introduction

There are numerous studies reporting the significant influence of the recent declining trend in Arctic sea-ice extent (Stroeve et al., 2012) on marine ecosystems (i.e., Grebmeier et al., 2010; Wassmann and Reigstad, 2011; Wassmann et al., 2011). In the Canada Basin of the western Arctic Ocean, the decrease in sea-ice cover results in deepening of the nutricline in the central part of the Beaufort Gyre (McLaughlin and Carmack, 2010; Nishino et al., 2011a). The intensification of sea-surface circulation promotes lateral shelf–basin interactions (Nishino et al., 2011b; Watanabe and Hasumi, 2009), which influence to ecosystems and biogeochemical cycles.

While the shelf and shelf slope areas of the Arctic Ocean have been substantially monitored (i.e., Hargrave et al., 1989; Fukuchi et al., 1993; Wassmann et al., 2004; Forest et al., 2007, 2011; Gaye et al., 2007; Sampei et al., 2011), the year-round study of sinking biogenic particles over the basins is still limited, except for a few studies (Fahl and Nöthig, 2007; Lallande et al., 2009; Honjo et al., 2010; O'Brien et al., 2013). In the cryopelagic Canada Basin, where the major primary producer is picoplankton, the biogenic particles are remineralized in the upper water column and particulate organic carbon (POC) supplied into the deep sea are essentially composed of allochthonous old carbon (Honjo et al., 2010). The low productivity of shell-bearing microplankton and zooplankton fecal pellets, which have a role as ballast for settling organic matter, limits the function of biological pump in the oligotrophic cryopelagic Canada Basin (Honjo et al., 2010). A long-term sediment trap experiment containing observation of diatom fluxes have been conducted in the Fram Strait (Bauerfeind et al., 2009). The only previous report on an annual time-series of diatom fluxes in the basin of the Arctic Ocean is that by Zernova et al. (2000), whose target region was at Station LOMO2 off the Laptev Sea. Zernova et al. (2000) showed high diatom production and high settling fluxes of diatom particles under sea-ice at Station LOMO2 during the seasonal maximum of solar radiation. Lallande et al. (2014) compared short-term monitoring data on diatom flux in the

Laptev Sea during 1995, Fram Strait in 1997, and central Arctic Ocean in 2012. They suggested that nutrient supply is the key factor for summer diatom production and POC flux in the central Arctic Basin. In the Chukchi Borderland, the ice-tethered drifting sediment trap "S97-120m" was deployed in 1998, and relatively high POC flux compared to that in the Canada Basin was observed (Honjo et al., 2010). Based on the first year-round monitoring of settling particle flux in the southern Northwind Abyssal Plain by Watanabe et al. (2014), it was suggested that the large amount of settling biogenic and lithogenic particles in November-December 2010 was transported from the Chukchi Sea shelf by the westward advection of cold eddy which developed around the off Barrow Canyon in early summer 2010. According to schematic diagram in Honjo et al. (2010), POC flux at ~120 m depth at 75°N and ~200 m depth at 80°N in the Canada Basin is about 10 and 7 mmol m^{-2} yr^{-1}, respectively. The annual POC flux at Station NAP for the first deployment period is about 27 and 20 mmol m^{-2} yr^{-1} at shallow and deep traps, respectively (Watanabe et al., 2014).

Diatom dominances in phytoplankton assemblages are usually observed in eutrophic waters whereas dominance of flagellates and picoplankton rather than diatoms are observed in oligotrophic waters such as central basin (Ardyna et al., 2011; Coupel et al., 2012; Lallande et al., 2014). Diatoms are one of the dominant phytoplankton in the Chukchi Sea (Sukhanova et al., 2009; Coupel et al., 2012; Joo et al., 2012; Laney and Sosik, 2014), and the recent environmental changes have influenced the diatom flora and phytoplankton phenology (Arrigo et al., 2012; Ardyna et al., 2014). As one of the major contributors to the biological pump, settling diatom fluxes in the offshore regions along the Chukchi Sea shelf are likely affected by the recent dramatic environmental changes.

In this paper, we present new findings on the settling flux of diatom valves and the relationships between diatom valve flux, sinking diatom flora, and upper water-mass properties in the southern Northwind Abyssal Plain from October 2010 to September 2012. The Chukchi Sea is one of the obvious areas of retreating summer sea-ice (Stroeve et al., 2012). The upper water column in the Chukchi Borderland can be affected by three characteristic water-masses: Pacific water, East Siberian Shelf water, and Beaufort Gyre water (Nishino et al., 2011a). Watanabe et al. (2014) documented the eddy-induced winter maximum of settling particle flux at Station NAP. This early-winter event should be observed in settling diatom flux. This paper newly mentions on the summer flux of settling diatom particles in addition to winter flux

93 maximum event of diatom flux. The present paper is the first report on year-round diatom floral
94 flux after the clear trend of declining sea-ice in the western Arctic Ocean. We expect that the
95 recent hydrographic changes in the western Arctic Ocean will be reflected in the settling diatom
96 flux and associated assemblages. The objectives of this paper are (1) to report the variation in
97 diatom flux and assemblage, and (2) to consider how hydrographic changes in the upper water
98 column are reflected in the diatom assemblage and diatom flux in the Northwind Abyssal Plain.
99
100 **2. Materials and methods**
101
102 Two year-round deployments of a bottom-tethered mooring with two conical
103 time-series sediment traps (model SMD26S-6000; Nichiyu Giken Kogyo Co. Ltd., Tokyo,
104 Japan) were conducted at Station NAP on the southern Northwind Abyssal Plain (75°N, 162°W;
105 1975-m water depth) from 4 October 2010 through 27 September 2011 and from 4 October
106 2011 through 17 September 2012. Sediment trap with pressure and temperature sensors was
107 deployed at shallow depth (about 180-260m) and deep depth (1300-1360m). The settling
108 particles were collected for 10–15 days per sample. Before sediment-trap deployment, the 26
109 sampling cups of each trap were filled with seawater containing 5% neutralized formalin as an
110 antiseptic (pH~8.2). In this study we analyzed the samples from both traps except the one that
111 contained a very low volume of trapped particles.
112 The recovered sediment-trap samples were sieved through a 1-mm mesh to remove
113 swimmers (Matsuno et al., 2014), and then the fine size-fraction (less than 1 mm) was split into
114 appropriate aliquots (1/1000) for diatom analysis by using a wet sample divider (WSD-10;
115 McLane Research Laboratories, East Falmouth, Massachusetts, USA). One of the aliquots was
116 filtered onto a membrane filter (0.45-μm pore size) with a 3-mm grid. The sample was desalted
117 by rinsing with Milli-Q water, and then the sample filter was dried overnight in an oven at 50 °C.
118 Two sample filters were prepared for each sample, and then one of the filters was mounted on a
119 microscope glass slide with Canada balsam.
120 Sample filters mounted on the glass slides were counted for diatoms under a light
121 microscope at 600× magnification. A duplicate sample was observed using scanning electron
122 microscope observation after osmium coating. A minimum of 400 diatom valves (including
123 resting-spore valves) per sample were identified, usually to species or genus level. Diatom

124 fluxes were estimated on the basis of valve counts, aliquot size, filtered area (535 mm^2), area of
125 sample filter observed, aperture area of sediment trap (0.5 m^2), and the sampling period
126 (Onodera et al., 2005). As described in a previous microplankton flux study in the southeastern
127 Beaufort Sea (Forest et al., 2007), the flux of diatom-derived POC (hereafter, diatom POC flux)
128 was estimated on the basis of diatom cell size and an equation for converting cell volume to
129 carbon content per diatom cell (Menden-Deuer and Lessard, 2000). The method for bulk
130 component analysis is described by Watanabe et al. (2014).
131 Sea-ice concentration and light intensity close to Station NAP during the sampling
132 period were obtained from the National Centers for Environmental Prediction (NCEP)/Climate
133 Forecast System Reanalysis (CFSR) (Saha et al., 2010). Sea surface temperature (SST) at
134 Station NAP was taken from the National Oceanographic and Atmospheric Administration
135 (NOAA) OI.v2 SST (Reynolds et al., 2002). Because the moored sediment trap array at Station
136 NAP did not include equipment to measure current velocity, and salinity, satellite-based sea ice
137 motion data and numerical simulation results from a physical oceanographic model known as
138 the Center for Climate System Research Ocean Component Model (COCO) (Hasumi, 2006)
139 were applied to estimate the sea ice and ocean current conditions in the western Arctic Ocean
140 during the sampling period. The National Snow and Ice Data Center (NSIDC) provided the
141 Polar Pathfinder 25 km EASE-Grid sea ice motion vectors, version 2 (Fowler et al., 2013). This
142 dataset was constructed from multiple satellite sensors, such as Special Sensor Microwave /
143 Imager (SSM/I), Advanced Microwave Scanning Radiometer-Earth Observing System
144 (AMSR-E), and Advanced Very High Resolution Radiometer (AVHRR), and in-situ
145 measurements of the International Arctic Buoy Programme (IABP). In our study, the monthly
146 mean vector data were downloaded from the NSIDC website
147 (http://nsidc.org/data/docs/daac/nsidc0116_icemotion.gd.html). The pan-Arctic ice-ocean model
148 has the horizontal grid size of about 25 km and 28 vertical levels, where the layer thickness
149 varies from 2 m in the uppermost level to 500 m below 1000 m depth. The sea ice part
150 includes a one-layer thermodynamic formulation (Bitz and Lipscomb, 1999) and
151 elastic-viscous-plastic rheology (Hunke and Dukowicz, 1997). The ocean component is a
152 free-surface ocean general circulation model formulated with the uniformly third-order
153 polynomial interpolation algorithm (Leonard et al., 1994) for horizontal advection
154 scheme. The model domain contains the entire Arctic Ocean, the

Greenland-Iceland-Norwegian seas, and the northern part of the North Atlantic. The spin-up experiment was initiated from the temperature and salinity fields of Polar Science Center Hydrographic Climatology version 3.0 (Steele et al., 2001), no ocean circulation, and no sea ice. The interannual experiment from 1979 to 2012 was then performed. Whereas most parts of experimental designs were the same as in Watanabe (2013) and Watanabe and Ogi (2013), the model version was upgraded from COCO 3.4 to 4.9 and the atmospheric forcing dataset was changed from NCEP1 (Kalnay et al., 1996) to the NCEP/CFSR in the present study.

3. Results

3.1 Oceanographic features and mooring conditions

Station NAP is located at the southwestern edge of the Beaufort Gyre (Fig. 1), and is occasionally influenced by relatively oligotrophic waters of the Beaufort Gyre (Nishino et al., 2011a). The study area is in polar night from early November through early February (Fig. 2a). The CFSR shortwave radiation at the sea surface (or surface of sea ice) ranged from 0 to 378 W m^{-2} (Fig. 2a). Station NAP is located in a seasonal sea-ice zone, and is covered by sea-ice from late October through July (Fig. 2b). Sea surface temperature temporarily increased to about 2 °C in early August in 2011 and 2012 (Fig. 2d).

The upper water column around the study area is categorized by four water masses (McLaughlin et al., 2011). Under the surface mixed layer (about the upper 25 m), Pacific summer water is observed at 25–100 m water depth (salinity approximately 31–32; Steele et al., 2004). Cold Pacific winter water (temperature minimum at 150 m, salinity around 33; Coachman and Barnes, 1961) is found under the Pacific summer water (100–250 m water depth). Higher salinity water originating from the Atlantic Ocean is observed under the Pacific winter water.

According to the logged data from pressure and temperature sensors attached to the sediment traps, the shallower sediment trap was moored at a water depth of 181–218 m (median, 184 m) for the first deployment period, and at 247–319 m (median, 256 m) for the second (Fig. 2c). Therefore, the shallow trap was in Pacific winter water during the sampling period, except

for in May and July 2012 (Fig. 2c, d). In July 2012, the depth of the shallower trap deepened to 320 m in the warm Atlantic water layer, probably because of intensified water currents and incline of mooring, which might have temporarily decreased the trapping efficiency for sinking particles (Matsuno et al., 2014). Although the deepening of shallow trap in May 2012 was minor compared to that in July 2012, the increase of water temperature at shallow trap depth suggests the shallowing upper boundary of the Atlantic water layer. The deeper sediment trap was moored at 1318–1378 m for the entire sampling period.

3.2 Total mass flux and bulk components

As previously reported by Watanabe et al. (2014), the total mass flux showed clear annual maxima in November–December in both 2010 and 2011 (Fig. 2e, f). The major component of trapped particles was lithogenic silt-clay minerals (Fig. 2e). There was another peak in total mass flux in summer 2011, but this summer peak did not appear in 2012. The time-series of biogenic opal flux showed variations similar to those of total mass flux (r = 0.93 for shallow trap data, n = 34) (Fig. 2e). Microscopic observation suggests that the biogenic opal in the studied material consisted mainly of diatom valves and radiolarian shells (Ikenoue et al., 2014). The trap samples also contained low numbers of silicoflagellate skeletons, siliceous endoskeleton of dinoflagellate genus *Actiniscus*, chrysophyte cysts, ebridian flagellate and palmales. The contribution of these siliceous flagellates to POC and biogenic opal fluxes appears minor compared to the contribution from diatoms and radiolarians. This result is different from a previous observation on the Mackenzie Shelf in the southwestern Beaufort Sea that showed a significant contribution by small flagellates to the POC flux (Forest et al., 2007).

3.3 Diatom valve flux and species composition

The total diatom flux captured in the shallow trap showed clear seasonality (Fig. 3a). A relatively high flux of diatom valves was observed in November–December 2010, August–September 2011, and November–December 2011 (Fig. 3a). The sinking diatom flux rapidly increased in August 2011, when the sea-ice retreated at Station NAP (Figs. 2b, 3a). The maximum of the total diatom flux at the shallow trap depth in summer 2011 reached 11.3 × 10^6

valves m^{-2} d^{-1} in the period from 18 to 31 August. This maximum was approximately 28% of the diatom flux maximum at Station LOMO2 (150-m trap depth) in summer 1996 (Zernova et al., 2000). In 2012, a seasonal increase in total diatom flux started after June. However, in contrast to summer 2011, there was no clear maximum of diatom flux as the same as low total mass flux in June–September 2012. The maximum fluxes reached 17.5×10^6 valves m^{-2} d^{-1} and 10.8×10^6 valves m^{-2} d^{-1} in early winter 2010 and 2011, respectively. The high diatom flux season at the deep trap was similar to that at the shallow trap (Fig. 3a, b). However, there was different between two traps that total diatom flux at deep trap in summer 2011 was higher than those in early winter maxima of 2010 and 2011.

The diatoms found in all samples examined were categorized into 98 taxa (Table 1). Because diatom species usually observed in fresh or low-salinity water were very rare, the biogenic materials collected in this study were primarily of marine origin. In the shallow trap samples, the genera *Thalassionema* and *Chaetoceros* (subgenus *Hyalochaete*) were the major components from late October 2010 to early July 2011 (Fig. 3c). *Chaetoceros* relatively increased in late November-December 2010. *Thalassionema* relatively increased in the low flux period and reached to 70% in March 2011. Then, t *Fragilariopsis (oceanica* and *cylindrus)*, which are sea ice-related diatom species (Ren et al., 2014), gradually increased from April to August 2011. The sinking diatom assemblage in summer 2011 was mainly composed of *Fossula arctica*, one of the common sea-ice diatoms in the Arctic Ocean (Cremer, 1999; Quillfeldt, 2003). The maximum relative abundance of *F. arctica* was 80% in 14-28 September 2011. After the period of *F. arctica* dominance, the relative abundance of *Proboscia eumorpha* increased in shallow trap samples in October-November 2011 (Fig. 3c).The sinking diatom flora during the high flux period of November–December 2011 was essentially the same as that in 2010, although the relative abundance of *Chaetoceros* resting spores was relatively minor compared to other diatoms (Fig. 3a, b). The relative increases of *Fragilariopsis* and *Fossula* were not observed in 2012. The relative abundance of sea ice-related diatoms was less than 23% in summer 2012. Instead, relative abundance of planktic diatoms such as *Thalassiosira* spp. and *Nitzschia* spp. increased in settling diatom assemblage in summer 2012.

In comparison of shallow and deep trap diatom floras, the dominant species in settling diatom flora of two traps were the same in the periods of diatom flux maxima (Fig. 3d). However, time-series succession of major diatom species in deep trap samples were unclear

compared to that of shallow trap. The clear increase in the relative abundance of *Proboscia* observed at shallow trap in October-November 2011 was not observed at deep trap

Melosira arctica, which was commonly observed at Station LOMO2 (Zernova et al., 2000) and under summer sea ice in the northern Laptev Sea (Lallande et al., 2014), was rarely observed in our samples (<2% numerical valve abundance). It has been reported that *Neodenticula seminae* is an endemic species in the subarctic North Pacific (Hasle, 1976; Yanagisawa and Akiba, 1990). This species has been expanding its distribution to the North Atlantic Ocean via the Arctic Ocean since 1999 (Reid et al., 2007). At Station NAP, *N. seminae* frustules and their fragments were sporadically observed in both shallow and deep trap samples (Fig. 3c, d). Some diatom valves were observed within aggregated clay minerals, which are considered an allochthonous component originating from the Chukchi Sea shelf.

3.4 Sinking speed

Using the time-lag between the observed flux maxima at the shallow and deep trap depths, we estimated the average sinking speed of aggregated diatom particles between these depths at 37–75 m d^{-1} in November 2010 and >85 m d^{-1} in August 2011. The faster sinking speed in August 2011 was primarily due to the abundant gelatinous material of zooplanktonic origin and the larger particle sizes resulting from chains of the diatoms *Fossula arctica* and *Fragilariopsis* spp.

3.5 Diatom POC flux

In order to estimate the diatom contribution to POC flux, the diatom POC flux is required instead of the flux data for diatom valve abundance. Time-series fluctuations in the diatom POC flux and in the dominant taxa in diatom POC estimation differ from those of the diatom valve flux because of the temporary increases in the flux of larger centric diatoms (Figs. 3 and 4). The estimated diatom POC flux is based on observed valve numbers. It is therefore difficult to estimate the influence of selective decomposition of diatom valves and diatom carbon on the POC flux during the sinking process. In November–December most of the POC

was attributed to *Coscinodiscus*, *Rhizosolenia*, and *Chaetoceros* (Fig. 4). A temporary increase in diatom POC flux was caused by the appearance of large *Coscinodiscus* in late March and from mid-April to early May 2011. The ice-related algae *Fossula arctica* was the primary species in diatom POC flux during August–September 2011. The high diatom POC flux from *Rhizosolenia* and *Proboscia* in November 2011 was evidenced by the abundant occurrence of the end parts of their needle-like valves rather than the abundant occurrence of intact cells. Thus, the diatom POC flux in November 2011 became overestimate and exceeded total POC flux. *Proboscia* was dominant in the eastern Chukchi Sea shelf waters in September–October 2010 (J. Onodera, unpublished data). The diatom POC flux in summer 2012 was composed mainly of *Thalassiosira* spp. Although vegetative *Chaetoceros* (subgenus *Hyalochaete*) and *Thalassionema* were numerically abundant, their contribution to diatom POC was relatively minor because their cell volume is one to five orders smaller than *Coscinodiscus*, *Rhizosolenia*, *Proboscia*, and *Thalassiosira*.

4. Discussion

4.1 Summer diatom flux and changes in upper water masses

Because the phytoplankton productivity and phytoplankton assemblage is clearly different between the Chukchi Sea shelf and the Canada Basin, the settling diatom flux at Station NAP should reflect the times-series hydrographic variations. The diatom flux and species composition observed in summer 2011 and 2012 probably reflected the dominance of different water masses—shelf water or oligotrophic Beaufort Gyre water—in the upper water column. The high dominance of *Fossula arctica* at Station NAP in summer 2011 suggests the presence of sea-ice transported from the highly productive Chukchi Sea shelf. This species is commonly observed in the spring assemblage of ice and water in the Chukchi Sea (Quillfeldt et al., 2003). According to data for the biogeographic diatom distribution in the Laptev Sea, *F. arctica* is mainly observed in the sea-ice assemblage around shelf zones rather than on the basin side (Cremer, 1999). The relatively high flux of lithogenic material in 2011 also suggests that many of the particles trapped in this study originated primarily from the Chukchi Sea shelf. During October 2010, there was a high cell density of *Proboscia eumorpha* over the eastern

310 Chukchi Sea shelf, whereas there was a low cell density of *Proboscia* species in water samples
311 from the southwestern Canada Basin and the Northwind Abyssal Plain (J. Onodera, unpublished
312 data). The relative increase in *P. eumorpha* after the period of *F. arctica* dominance in 2011
313 probably suggests the influence of Chukchi shelf waters on Station NAP. The transport of
314 coastal water toward Station NAP in summer 2011 was also inferred from the trapped Pacific
315 copepod *Neocalanus cristatus* (Matsuno et al., 2014). Abundant gelatinous zooplankton material,
316 such as "houses" of appendicularian Oikopleuridae (S. Chiba, pers. comm.), was also observed
317 in August-September 2011. In contrast to the situation in 2011, the limited influence of
318 shelf-origin sea-ice and shelf waters around Station NAP in 2012 are evidenced by the absences
319 of biogenic and lithogenic particle fluxes and the rare occurrences of *F. arctica* and other coastal
320 biogenic particles in January–September 2012.
321 To examine the background mechanisms for the suppressed biogenic fluxes in summer 2012,
322 we addressed the relationship between horizontal advection and settling particle fluxes using the
323 satellite-based sea ice motion data and the pan-Arctic ice–ocean model. The sea ice and water
324 mass properties at Station NAP should be considered to be occasionally influenced by
325 inter-annual variability in the Beaufort Gyre circulation. First, we checked the Polar Pathfinder
326 sea ice motion vectors. The seasonal averages in the western Arctic Ocean were plotted in Fig. 5.
327 During the winter season from November 2010 to January 2011, an anti-cyclonic sea ice
328 circulation (normally called as Beaufort Gyre) appeared over the Canada Basin and Chukchi
329 Borderland. This pattern subsided once in early spring and was then recovered for the summer
330 season from May to July 2011. Thus the source region of sea ice around Station NAP would
331 have been the southern Beaufort Sea in 2011. On the other hand, southward sea ice motion
332 prevailed from winter to spring 2012. The anti-cyclonic circulation was shown in following
333 early summer, but its strength was clearly weaker than 2011. The difference between two years
334 also indicated that shelf-origin sea ice less affected settling particle fluxes around Station NAP
335 in 2012.
336 Next, we analyzed the results from our inter-annual experiment using the 25-km grid COCO
337 model. The spatial pattern of simulated sea ice motion was nearly consistent with the
338 satellite-based one (Fig. 6). We then compared the simulated sea-surface height in the western
339 Arctic Ocean using the summertime averages in 2011 and 2012 (Fig. 7). In general, the spatial
340 pattern of sea surface height reflects the intensity and location of the oceanic Beaufort Gyre.

341 The COCO model demonstrated that the sea-surface height was higher over the entire western
342 Arctic basin and the maximum height was located more to the western side of the basin in
343 summer 2012 than those in summer 2011. This difference between the two years indicates that
344 the Beaufort Gyre expanded toward the Chukchi Borderland in 2012.
345 The five-year time-series of simulated ocean current direction in the surface 100-m layer
346 shows that a northwestward current frequently prevailed east of Station NAP (Fig. 8). This
347 situation favors the spread of shelf-origin water with high abundance of coastal diatom taxa and
348 lithogenic materials toward the Chukchi Borderland. The model results also show that the
349 current direction switched southwestward in December 2011. Because the central Canada Basin
350 is known as an oligotrophic region (Nishino et al., 2011a), the transport of nutrient-poor basin
351 water toward Station NAP would be a possible factor for explaining the lower diatom flux in
352 summer 2012. These model results suggest that variations in the Beaufort Gyre significantly
353 influenced nutrient availability and the consequent biogenic fluxes at Station NAP.
354
355 **4.2 Lateral advection of coastal diatoms in early winter**
356
357 Based on biogeographic characteristics, much of the *Chaetoceros* resting spores and
358 other coastal diatoms in the studied samples can be regarded as allochthonous materials
359 transported from shelf to basin. Compared to previous studies of particulate carbon fluxes in the
360 Arctic Ocean (summarized in Wassmann et al., 2004), the early winter maximum of POC flux in
361 our study is unusual under conditions of sea-ice cover and polar night. No diatom flux
362 maximum was observed in any early winter during the previous diatom flux study at Station
363 LOMO2 (Zernova et al., 2000). Because polar diatoms show tolerance to low light intensity
364 (Lee et al., 2008), the autumn diatom production probably continued under sea-ice cover and
365 decreasing solar radiation at Station NAP after late October (Fig. 2a, b). However, the high
366 diatom production and subsequent flux of settling diatoms and other biogenic particles,
367 comparable to the summer situation, cannot be explained on the basis of the general seasonality
368 of primary production and sinking particle flux in the seasonal sea-ice zone of the Arctic Ocean
369 (Wassmann et al., 2004; Wassmann and Reigstad, 2011). In this study, we also observed the
370 annual maximum of lithogenic particle flux during the period of the high flux of sinking
371 diatoms in November–December (Figs. 2 and 3; Watanabe et al., 2014). In the early winter of

each year, the origin of diatom particles comprising the diatom flux maximum around Station NAP should be treated as a complex of transported shelf-origin materials and autochthonous diatoms. The dominance of *Chaetoceros* (subgenus *Hyalochaete*) spp. and their resting spores, and abundant silt-clay minerals in the studied samples, suggests the substantial influence of Chukchi Sea shelf waters.

The increased supply of coastal diatoms and lithogenic materials in early winter can be explained by several possible mechanisms for their transport from shelf to basin. Re-suspension of shelf bottom materials into the upper water column would cause the continuous dominance of lithogenic materials with coastal diatom valves in the studied particles at Station NAP. In addition, suspended neritic diatoms are incorporated into sea ice and driven offshore (Różańska et al., 2008). However, sea-ice drift and the usual re-suspension of shelf materials cannot fully explain the early winter flux maxima of diatoms and lithogenic particles at Station NAP. The high-resolution pan-Arctic Ocean model COCO demonstrated that a drifting anti-cyclonic cold eddy generated north of Point Barrow in June 2010 passed Station NAP at the 100- to 200-m water depth during late October–early December 2010 (Watanabe et al., 2014). The simulated cold eddy passage was consistent with the observed event-like cooling and deepening of the moored trap depth that we recorded in late October–December 2010 (Fig. 2c, d). In addition, this eddy continued to pull cold water from the outer shelf during the early part of its passage from off Point Barrow toward Station NAP. Therefore, the movement of the cold eddy could account for the appearance of the high proportion of shelf bottom-water at Station NAP in late October–early December (Fig. S2.2 in Watanabe et al., 2014).

Based on the observed characteristics of diatom floral fluxes and the physical oceanographic simulation, we suggest that the early-winter maximum of diatom flux observed in this study is primarily caused by a drifting cold eddy that developed along the shelf break off Point Barrow (Watanabe et al., 2014). The smaller maximum of diatom flux at deep trap in early winter is probably reflecting the horizontal diffusion of settling particles in deep layer under eddy (Siegel et al., 1990) in addition to biogenic particle decomposition. Whereas eddy-induced lateral transport of coastal materials has been reported in the Canada Basin (O'brien et al., 2011, 2013; Nishino et al., 2011b), the eddy in this study, composed of Pacific-origin waters with lower density, did not flow down the shelf slope. Because the shallow sediment trap was moored at about 260 m during the second deployment, the direct influence of the cold eddy was

not detected by the temperature and pressure sensors attached to the sediment trap. However, a similar eddy-induced transport event of shelf materials to the basin in early winter 2011 is evident in the high diatom flux, the characteristic diatom assemblage, and the high abundance of lithogenic clay particles.

4.3 Role of diatoms in the biological pump

Because biogenic opal has a ballast effect on the export of particulate organic matter to deep basins (Honjo et al., 2008; Honda and Watanabe 2010), the biological pump is usually effective in diatom-rich oceans such as the Aleutian Basin in the Bering Sea (Takahashi et al., 2002), the subarctic North Pacific (Honda et al., 2002; Takahashi et al., 2002; Honda and Watanabe, 2010), and the Southern Ocean (Honjo et al., 2008). However, most settling autochthonous POC in the central Canada Basin is remineralized within subsurface layers (Honjo et al., 2010). Fresh POC is not supplied to deeper layers, even though there is primary production of 2–4 mol C m^{-2} y^{-1} (Honjo et al., 2010). The primary producers in the cryopelagic Canada Basin are mainly green algae and other picoplankton (e.g., Coupel et al., 2012). The limited amounts of diatoms supplying biogenic ballast and fecal pellets are the causes of an ineffective biological pump in the Canada Basin (Honjo et al., 2010). The relatively abundant POC fluxes at Station NAP, in comparison to those at the subsurface and sediment-trap Station CD04-3067m (trap depth: 3067 m) in the central Canada Basin (Honjo et al., 2010), re due to the higher lateral carbon transport from the Chukchi Sea shelf, autochthonous production of phyto- and zooplankton around Station NAP (Watanabe et al., 2014).

The diatoms collected in our samples sometimes retained the chain form of frustules. In particular, frustules with residual protoplasm were also observed in the summer samples. Their occurrence suggests that the carbon supplied to the deep sea in the Northwind Abyssal Plain includes not only old carbon transported from the shelf or sea-floor ridge but also fresh carbon produced around the study area. When the influence of shelf-origin water is obvious at Station NAP, as in 2011, the biological pump at Station NAP will be relatively active owing to abundant supplies of biogenic and lithogenic particles. In contrast, when oligotrophic water from the central Canada Basin was supplied to Station NAP, as observed in early 2012, the sinking particle flux at Station NAP was limited. In this situation, the efficiency of the

biological pump might be reduced to a level comparable to that in the central Canada Basin. Therefore, on the Chukchi shelf side of the outer Beaufort Gyre, primary productivity and the biological pump are influenced by the spatial distribution of upper water masses (Nishino et al., 2011a). When oligotrophic sea-surface waters reduce the summer particle flux, as evident in summer 2012, the eddy effect on lateral advection of shelf materials to the basin (Nishino et al., 2011b; O'Brien et al., 2011, 2013; Watanabe et al. 2014) becomes important to the seasonality of organic matter flux and the composition of the sinking microplankton flora in the study area (Watanabe et al., 2014).

Author contributions

N.H. planned the research project. J.O. carried out the diatom analysis and offshore work of sediment-trap mooring experiments. E.W. implemented the physical oceanographic model. M.C.H. analyzed the biogenic opal in sediment trap samples. J.O. and E.W. prepared the manuscript with contributions from all co-authors.

Acknowledgements

We gratefully thank the captains, crews, chief scientist and marine technicians of R/V *Mirai* and I/B CCGS *Sir Wilfrid Laurier* for mooring operations, Dr. Takashi Kikuchi for cruise logistics, and Dr. Yuichiro Tanaka for supplying sediment trap equipment. This work was funded a Grant-in-Aid for Scientific Research (S) of the Japan Society for the Promotion of Science (JSPS) JFY2010-2014, No. 22221003, "Catastrophic reduction of sea ice in the Arctic Ocean: its impact on the marine ecosystems in the polar region" to N.H., and by a JSPS Research Fellowship for Young Scientists to J.O. (No. 22-5808). Modeling experiments were executed by E.W. using the Japan Agency for Marine-Earth Science and Technology (JAMSTEC) Earth Simulator version 2.

References

Arrigo, K. R., Perovich, D.K., Pickart, R. S., Brown, Z. W., van Dijken, G. L., Lowry, K. E., Mills, M. M., Palmer, M. A., Balch, W. M., Bahr, F., Bates, N. R., Benitez-Nelson, C., Bowler, B., Brownlee, E., Ehn, J. K., Frey, K. E., Garley, R., laney, S. R., Lubelczyk, L, Mathis, J., Matsuoka, A., Mitchell, B. G., Mooore, W. K., Ortega-Retuerta, E., Ppal, S.,

Polashenski, C. M., Reynolds, R.A., Schieber, B., Sosik, H. M., Stephens, M., and Swift, J. H.: Massive phytoplankton blooms under Arctic sea ice. Science, 336, 1408, doi: 10.1126/science.1215065, 2012.

Ardyna, M., Gosselin, M., Michel, C., Poulin, M., and Tremblay, J-É.: Environmental forcing of phytoplankton community structure and function in the Canadian High Arctic: contrasting oligotraphic and eutrophic regions. Mar. Ecol. Prog. Ser., 442, 37-57, 2011.

Ardyna, M., Babin, M., Gosselin, M., Devred, E., Rainville, L., and Tremblay, J-É.: Recent Arctic Ocean sea ice loss triggers novel fall phytoplankton blooms. Geophys. Res. Lett., 41, 6207-6212, 2014.

Bauerfeind, E., Nöthig, E-M., Beszczynska, A., Fahl, K., Kaleschke, L., Kreker, K., Klages, M, Soltwedel, T., Lorenzen, C., and Wegner, J.: Particle sedimentation patterns in the eastern Fram Strait during 2000-2005: Results from the Arctic long-term observatory HAUSGARTEN. Deep-Sea Res. I, 56, 1471-1487, 2009.

Bitz, C. M. and Lipscomb, W. H.: An energy-conserving thermodynamic model of sea ice, J. Geophys. Res., 104, 15,669-15,677, 1999.

Boetius, A., Albrecht, S., Bakker, K., Bienhold, C., Felden, J., Fernández-Méndez, M., Hendricks, S., Katlein, C., Lalande, C., Krumpen, T., Niclaus, M., Peeken, I., Rabe, B., Rogacheva, A., Rybakova, E., Somavilla, R., Wenzhöfer, F., and RV Polarstern ARK27-3-Shipboard Science Party.: Export of algal biomass from the melting Arctic sea ice. Science, 339, 1430–1432, doi: 10.1126/science.1231346, 2013.

Coachman, L. K. and Barnes, C. A.: The contribution of Bering Sea water to the Arctic Ocean. Arctic, 14, 147–161, 1961.

Coupel, P., Jin, H. Y., Joo, M., Horner, R., Bouvet, H. A., Sicre, M. –A., Gascard, J. –C., Chen, J. F., Garçon, and Ruiz-Pino, D.: Phytoplankton distribution in unusually low sea ice cover over the Pacific Arctic. Biogeosci., 9, 4835–4850, doi: 10.5194/bg-9-4835-2012, 2012.

Cremer, H.: Distribution patterns of diatom surface sediment assemblages in the Laptev Sea (Arctic Ocean). Marine Micropaleontol., 38, 39-67, 1999.

Danielson, S., Curchitser, E., Hedstrom, K., Weingartner, T., and Stabeno, P.: On ocean and sea ice modes of variability in the Bering Sea. J. Geophys. Res., 116, C12036, doi:10.1029/2011JC007389, 2011.

Fahl, K. and Nöthig, E. -M.: Lithogenic and biogenic particle fluxes on the Lomonosov Ridge

(central Arctic Ocean) and their relevance for sediment accumulation: Vertical vs. lateral transport. Deep-Sea Res. pt. I, 54, 1256–1272, 2007.

Forest, A., Sampei, M., Hattori, H., Makabe, R., Sasaki, H., Fukuchi, M., Wassmann, P., and Fortier, L.: Particulate organic carbon fluxes on the slope of the Mackenzie Shelf (Beaufort Sea): Physical and biological forcing of shelf-basin exchanges. J. Mar. Sys., 68, 39–54, 2007.

Forest, A., Galindo, V., Darnis, G., Pineault, S., Lalande, C., Tremblay, J-E., and Fortier, L.: Carbon biomass, elemental ratios (C:N) and stable isotopic composition ($\delta^{13}C$, $\delta^{15}N$) of dominant calanoid copepods during the winter-to-summer transition in the Amundsen gulf (Arctic Ocean). J. Plankton Res., 33, 161–178, 2011.

Fowler, C., Emery, W., and Tschudi, M.: Polar Pathfinder Daily 25 km EASE-Grid Sea Ice Motion Vectors. Version 2. Boulder, Colorado USA: National Snow and Ice Data Center, 2013.

Fukuchi, M., Sasaki, H., Hattori, H., Matuda, O, Tanimura, A., Handa, N., and McRoy, C. P.: Temporal variability of particulate flux in the northern Bering Sea. Cont. Shelf Res., 13, 693–704, 1993.

Gaye, B., Fahl, K., Kodina, L. A., Lahajnar, N., Nagel, B., Unger, D., and Gebhardt, A. C.: Particulate matter fluxes in the southern and central Kara Sea compared to sediments: Bulk fluxes, amino acids, stable carbon and nitrogen isotopes, sterols and fatty acids. Cont. Shelf Res., 27, 2570–2594, 2007.

Grebmeier, J. M., Moore, S. E., Overland, J. E., Frey, K. E., and Gradinger, R.: Biological response to recent Pacific Arctic sea ice retreats. Eos, 91, 161–162, 2010.

Hunke, E. C. and Dukowicz, J. K.: An elastic-viscous-plastic model for sea ice dynamics. J. Phys. Oceanogr., 27, 1849–1867, 1997.

Hargrave, B. T., von Bodungen, B., Conover, R. J., Fraser, A. J., Phyllips, G., and Vass, W. P.: Seasonal changes in sedimentation of particulate matter and lipid content of zooplankton collected by sediment trap in the Arctic Ocean off Axel Heiberg Island. Polar Biol., 9, 467–475, 1989.

Hasle, G. R.: The biogeography of some marine planktonic diatoms. Deep-Sea Res., 23, 319–338, 1976.

Hasumi, H.: CCSR Ocean Component Model (COCO) version 4.0. Center for Clim. Sys. Res.

Rep., Univ. of Tokyo, 25, 1–103, 2006.

Honda, M. C. and Watanabe, S.: Importance of biogenic opal as ballast of particulate organic carbon (POC) transport and existence of mineral ballast-associated and residual POC in the Western Pacific Subarctic Gyre. Geophys. Res. Lett., 37, L02605, doi: 10.1029/2009GL041521, 2010.

Honda, M. C., Imai, K., Nojiri, Y., Hoshi, F., Sugawara, T., and Kusakabe, M.: The biological pump in the northwestern North Pacific based on fluxes and major components of particulate matter obtained by sediment-trap experiments (1997-2000). Deep-Sea Res. pt. II, 49, 5595–5625, 2002.

Honjo, S., Manganini, S. J., Krishfield, R. A., and Francois, R.: Particulate organic carbon fluxes to the ocean interior and factors controlling the biological pump: A synthesis of global sediment trap programs since 1983. Prog. Oceanogr., 76, 217–285, 2008.

Honjo, S., Krishfield, R. A., Eglinton, T. I., Manganini, S. J., Kemp, J. N., Doherty, K., Hwang, J., McKee, T. K., and Takizawa, T.: Biological pump processes in the cryopelagic and hemipelagic Arctic Ocean: Canada Basin and Chukchi Rise. Prog. Oceanogr., 85, 137–170, 2010.

Ikenoue, T., Bjørklund, K. R., Kruglikova, S. B., Onodera, J., Kimoto, K., and Harada, N.: Flux variations and distributions of microzooplankton (Radiolaria) in the western Arctic Ocean: environmental indices in a warming Arctic. Biogeosciences Discuss., 11, 16645-16701, 2014.

Joo, H.M., Lee, S.H., Jung, S.W., Dahms, H-U., and Lee, J.H.: Latitudinal variation of phytoplankton communities in the western Arctic Ocean. Deep-Sea Res. II, 81-84, 3-17, 2012.

Kalnay, E., et al.: The NCEP/NCAR 40-year reanalysis project. Bull. Amer. Meteor. Soc. 77, 437-471, 1996.

Lallande, C., Bélanger, S., Fortier, L.: Impact of a decreasing sea ice cover on the vertical export of particulate organic carbon in the northern Laptev Sea, Siberian Arctic Ocean. Geohys. Res. Lett., 36, L21604, 2009. doi:10.1029/2009GL040570

Lallande, C., Nöthig, E-M., Somavilla, R., Bauerfeind, E., Shevchenko, V., Okolodkov, Y.: Variability in under-ice export fluxes of biogenic matter in the Arctic Ocean. Global Biogeochem. Cycles, 28, 571-583, 2014. doi:10.1002/2013GB0004735.

Laney, S.R., Sosik, H.M.: Phytoplankton assemblage structure in and around a massive under-ice bloom in the Chukchi Sea. Deep-Sea Res. II, 105, 30-41, 2014.

Lee, S. H., Whitledge, T. E., and Kang, S. H.: Carbon uptake rates of sea ice algae and phytoplankton under different light intensities in a landfast sea ice zone, Barrow, Alaska. Arctic, 61, 281–291, 2008.

Leonard, B. P., MacVean, M. K., Lock, A. P.: The flux-integral method for multi-dimensional convection and diffusion. NASA Tech. Memo. 106679, ICOMP-94-13, 1994.

Lowry, K. E., van Dijken, G. L., and Arrigo, K. R.: Evidence of under-ice phytoplankton blooms in the Chukchi Sea from 1998 to 2012. Deep-Sea Res. pt. II, 105, 105–117, 2014.

Matsuno, K., Yamaguchi, A., Fujiwara, A., Onodera, J., Watanabe, E., Imai, I., Chiba, S., Harada, N., and Kikuchi, T.: Seasonal changes in mesozooplankton swimmers collected by sediment trap moored at a single station on the Northwind Abyssal Plain in the western Arctic Ocean. J. Plankton Res., 36, 490–502, 2014.

McLaughlin, F., Carmack, E., Proshutinsky, A., Krishfield, R. A., Guay, C., Yamamoto-Kawai, M., Jackson, J. M., and Williams, B.: The rapid response of the Canada Basin to climate forcing: From bellwether to alarm bells. Oceanography, 24, 146–159, 2011.

McLaughlin, F.A., and Carmack, E.C.: Deepening of the nutricline and chlorophyll maximum in the Canada Basin interior, 2003-2009. Geophys. Res. Lett., 37, L24602, 2010. doi:10.1029/2010GL045459

Menden-Deuer, S. and Lessard, E. J.: Carbon to volume relationships for dinoflagellates, diatoms, and other protist plankton. Limnol. Oceanogr., 45, 569–579, 2000.

Nishino, S., Kikuchi, T., Yamamoto-Kawai, M., Kawaguchi, Y., Hirawake, T., and Itoh, M.: Enhancement/reduction of biological pump depends on ocean circulation in the sea-ice reduction regions of the Arctic Ocean. J. Oceanogr., 67, 305–314, 2011a.

Nishino, S., Itoh, M., Kawaguchi, Y., Kikuchi, T., and Aoyama, M.: Impact of an unusually large warm-core eddy on distributions of nutrients and phytoplankton in the southwestern Canada Basin during late summer/early fall 2010. Geophys. Res. Lett., 38, L16602, doi:10.1029/2011GL047885, 2011b.

O'Brien, M. C., Melling, H., Pedersen, T. F., and Macdonald, R. W.: The role of eddies and energetic ocean phenomena in the transport of sediment from shelf to basin in the Arctic. J. Geophys. Res., 116, C08001, doi:10.1029/2010JC006890, 2011.

O'Brien, M.C., Melling, H., Pedersen, T. F., and Macdonald, R. W.: The role of eddies on particle flux in the Canada Basin of the Arctic Ocean. Deep-Sea Res., pt. I, 71, 1–20, 2013.

Onodera, J., Takahashi, K., and Honda, M.C.: Pelagic and coastal diatom fluxes and the environmental changes in the northwestern North Pacific during December 1997-May 2000. Deep-Sea Res. II, 52, 2218-2239, 2005.

Passow, U. and Carlson, C. A.: The biological pump in a high CO_2 world. Mar. Ecol. Prog. Ser., 470, 249–271, 2012.

Quillfeldt, C.H. von, Ambrose, W.G.Jr., and Clough, L.M.: High number of diatom species in first-year ice from the Chukchi Sea. Polar Biol., 26, 806-818, 2003.

Reid, P. C., Johns, D. G., Edwards, M., Starr, M., Poulin, M., and Snoeijs, P.: A biological consequence of reducing Arctic ice cover: arrival of the Pacific diatom *Neodencitula seminae* in the North Atlantic for the first time in 800 000 years. Gl. Ch. Biol., 13, 1910–1921, 2007.

Ren, J., Gersonde, R., Esper, O., and Sancetta, C.: Diatom distributions in northern North Pacific surface sediments and their relationship to modern environmental variables. Palaeogeogr. Palaeoclimatol. Palaeoecol., 402, 81–103, 2014.

Reynolds, R. W., Rayner, N. A., Smith, T. M., Stokes, D. C., and Wang, W.: An improved in situ and satellite SST Analysis for climate. J. Climate, 15, 1609–1625, 2002.

Różańska, M., Poulin, M., and Gosselin, M.: Protist entrapment in newly formed sea ice in the Coastal Arctic Ocean. J. Mar. Sys., 74, 887–901, 2008.

Saha, S., Moorthi, S., Pan, H-L., Wu, X., Wang, J., Nadiga, S., Tripp, P., Kistler, R., Woollen, J., Behringer, D., Liu, H., Stokes, D., Grumbine, R., Gayno, G., Wang, J., Hou, Y-T., Chuang, H., Juang, H-M. H., Sela, J., Iredell, M., Treadon, R., Kleist, D., Delst, P. V., Keyser, D., Derber, J., Ek, M., Meng, J., Wei, H., Yang, R., Lord, S., van den Dool, H., Kumar, A., Wang, W., Long, C., Chelliah, M, Xue, Y., Huang, B., Schemm, J-K., Ebisuzaki, W., Lin, R., Xie, P., Chen, M., Zhou, S., Higgins, W., Zou, C-Z., Liu, Q., Chen, Y., Han, Y., Cucurull, L., Reynolds, R. W., Rutledge, G., and Goldberg, M.: The NCEP Climate Forecast System Reanalysis. Bull. Amer. Meteor. Soc., 91, 1015–1057, 2010.

Sampei, M., Sasaki, H., Makabe, R., Forest, A., Hattori, H., Tremblay, J-E., Gratton, Y., Fukuchi, M., and Fortier, L.: Production and retention of biogenic matter in the southeast Beaufort

620 Sea during 2003-2004: insights from annual vertical particle fluxes of organic carbon and
621 biogenic silica. Polar Biol., 34, 501–511, 2011.
622 Steele, M., Morley, R., Ermold, W.: PHC: A global ocean hydrography with a high-quality
623 Arctic Ocean. J. Climate, 14, 2079-2087, 2001.
624 Steele, M., Morison, J., Ermold, W., Rigor, I., Ortmeyer, M., and Shimada, K.: Circulation of
625 summer Pacific halocline water in the Arctic Ocean. J. Geophys. Res., 109, C02027,
626 doi:10.1029/2003JC002009, 2004.
627 Stroeve, J. C., Serreze, M. C., Holland, M. M., Kay, J. E., Malanik, J., and Barrett, A. P.: The
628 Arctic's rapidly shrinking sea ice cover: a research synthesis. Clim. Ch., 110, 1005–1027,
629 doi:10.1007/s10584-011-0101-1, 2012.
630 Sukhanova, I. N., Flint, M. V., Pautova, L. A., Stockwell, D. A., Grebmeier, J. M., and
631 Sergeeva, V. M.: Phytoplankton of the western Arctic in the spring and summer of 2002:
632 Structure and seasonal changes. Deep-Sea Res. II, 56, 1223-1236, 2009.
633 Takahashi, K., Fujitani, N., and Yanada, M.: Long term monitoring of particle fluxes in the
634 Bering Sea and the central subarctic Pacific Ocean, 1990-2000. Prog. Oceanogr., 55,
635 95–112, 2002.
636 Wang, J., Hu, H., Goes, J., Miksis-Olds, J., Mouw, C., D'Sa, E., Gomes, H., Wang, D. R.,
637 Mizobata, K., Saitoh, S., and Luo, L.: A modeling study of seasonal variations of sea ice
638 and plankton in the Bering and Chukchi Seas during 2007-2008. J. Geophys. Res. C
639 Oceans, 118, 1–14, doi:10.1029/2012JC008322, 2013.
640 Wassmann, P. and Reigstad, M.: Future Arctic Ocean seasonal ice zones and implications for
641 pelagic-benthic coupling. Oceanogr., 24, 220–231, 2011.
642 Wassmann, P., Bauerfeind, E., Fortier, M., Fukuchi, M., Hargrave, B., Moran, B., Noji, T.,
643 Nöthig, E.-M., Olli, K., Peinert, R., Sasaki, H., and Shevchenko, V.: Particulate organic
644 carbon flux to the Arctic Ocean sea floor, in: The organic carbon cycle in the Arctic
645 Ocean, edited by: Stein, R. and Macdonald, R. W., Berlin, Springer, 101–138, 2004.
646 Wassmann, P., Duarte, C. M., Agust, S., Sejr, M. K.: Footprints of climate change in the Arctic
647 marine ecosystem. Glob. Ch. Biol., 17, 1235–1249, doi:
648 10.1111/j.1365-2486.2010.02311.x, 2011.
649 Watanabe, E.: Linkages among halocline variability, shelf-basin interaction, and wind regimes
650 in the Beaufort Sea demonstrated in pan-Arctic Ocean modeling framework. Ocean

651 Model., 71, 43–53, doi:10.1016/j.ocemod.2012.12.010, 2013.
652 Watanabe, E. and Hasumi, H.: Pacific water transport in the western Arctic Ocean simulated by
653 an eddy-resolving coupled sea ice-ocean model. J. Phys. Oceanogr., 39, 2194–2211,
654 2009.
655 Watanabe, E. and Ogi, M.: How does Arctic summer wind modulate sea ice-ocean heat balance
656 in the Canada Basin? Geophys. Res. Lett., 40, 1569–1574, doi:10.1002/grl.50363, 2013.
657 Watanabe, E., Onodera, J., Harada, N., Honda, M. C., Kimoto, K., Kikuchi, T., Nishino, S.,
658 Mtsuno, K., Yamaguchi, A., Ishida, A., and Kishi, M. J.: An enhanced role of eddies in
659 the Arctic marine biological pump. Nat. Commun., 5, 3950, doi: 10.1038/ncomms4950,
660 2014.
661 Yanagisawa, Y. and Akiba, F.: Taxonomy and phylogeny of the three marine diatom genera,
662 *Crucidenticula, Denticulopsis* and *Neodenticula*. Bull. Geol. Surv. Japan, 41, 197–301,
663 1990.
664 Yun, M. S., Chung, K. H., Zimmermann, S., Zhao, J., Joo, H. M., and Lee, S. H.: Phytoplankton
665 productivity and its response to higher light levels in the Canada Basin. Polar Biol., 35,
666 257–268, doi: 10.1007/s00300-011-1070-6, 2012.
667 Zernova, V. V., Nöthig, E.-M., and Shevchenko, V. P.: Vertical microalga flux in the Northern
668 Laptev Sea (from the data collected by the yearlong sediment trap). Oceanology, 40,
669 801–808, 2000.
670
671

672 Table and figure captions

673

674 Table 1. Diatom taxa found in sediment trap samples from Station NAP collected from 4
675 October 2010 to 18 September 2012. The symbols "*" and "?" indicate sea ice-related
676 taxa, and uncertain identification in this study, respectively.

677

678 Figure 1. Bathymetric map around Station NAP (solid black circle at 75°N, 162°W) in the
679 western Arctic Ocean, and schematic of sea-surface circulation over the Chukchi Sea
680 shelf and in the southern Canada Basin (Danielson et al., 2011). NR, Northwind Ridge;
681 NAP, Northwind Abyssal Plain; CP, Chukchi Plateau; CS, Chukchi Spur; CAP, Chukchi
682 Abyssal Plain; AMR, Alpha-Mendeleev Ridge complex.

683

684 Figure 2. Time-series data at Station NAP from 1 October 2010 through 18 September 2012. (a)
685 Climate Forecast System Reanalysis (CFSR) reanalysis data of shortwave radiation, (b)
686 CFSR reanalysis data of sea-ice concentration, (c) depth log of moored shallow trap, (d)
687 water temperature recorded at moored shallow trap (black line), and NOAA OI.v2
688 weekly sea-surface temperature at Station NAP (gray line), (e) total mass flux and bulk
689 components of sinking particles at shallow trap depth (data period was expanded from
690 Watanabe et al., 2014), and (f) total mass flux and bulk components at deep trap depth.
691 Blank areas in bulk component data indicate no analysis because of limited sample
692 volume.

693

694 Figure 3. Total diatom flux and settling diatom assemblage at Station NAP from 4 October 2010
695 through 17 September 2012. (a) Sinking diatom flux at shallow trap, (b) sinking diatom
696 flux at deep trap, (c) relative diatom valve abundance excluding *Chaetoceros* spores at
697 shallow trap, and (d) relative diatom valve abundance excluding *Chaetoceros* spores at
698 deep trap. Blanks in time-series data indicate periods with no data because of limited
699 sample volume or periods without sampling because of mooring turnaround. The plot
700 data is listed in Table A1.

701

702 Figure 4. Time-series fluxes of total POC and diatom-derived carbon at Station NAP. (a)

703 Shallow trap, and (b) deep trap.
704
705 Figure 5. Sea ice motion vectors in the western Arctic Ocean derived from the Polar Pathfinder
706 dataset in (a-c) 2011 and (e-f) 2012. (g-i) Their difference (2012 minus 2011). Seasonal
707 averages for (a,d,g) November to January, (b,e,h) February to April, and (c,f,i) May to
708 July were calculated from monthly mean data. Each vector in the EASE grid was
709 interpolated to the COCO model grid for comparison, and the obtained vectors are shown
710 every eight grid (approximately 200 km). Unit vector corresponds to 5 cm s^{-1}. The
711 location of Station NAP is presented by the red circular symbol. Thin contours indicate
712 isobaths of 100 m, 1000 m, and 3000 m.
713
714 Figure 6. Same as Figure 5, but the COCO model result.
715
716 Figure 7. Sea surface height (cm) in the western Arctic Ocean obtained from the COCO model.
717 The summertime averages over June, July, and August are shown for (a) 2011 and (b)
718 2012. Black contours trace isobaths of 100 m, 1000 m, and 3000 m. The white contours
719 indicate a sea surface height of zero. The purple line corresponds to 75°N, used for
720 modeled current direction in Figure 8. Red dots show the location of Station NAP. Purple
721 dots represent the east and west limits of the horizontal section in Figure 8.
722
723 Figure 8 Modeled ocean current direction averaged from the surface to 100-m depth across an
724 east–west section along 75°N (see purple line in Figure 7). The vertical axis represents an
725 inter-annual time-series from 2008 to 2012. Blue (red) color indicates a northwestward
726 (southwestward) ocean current.

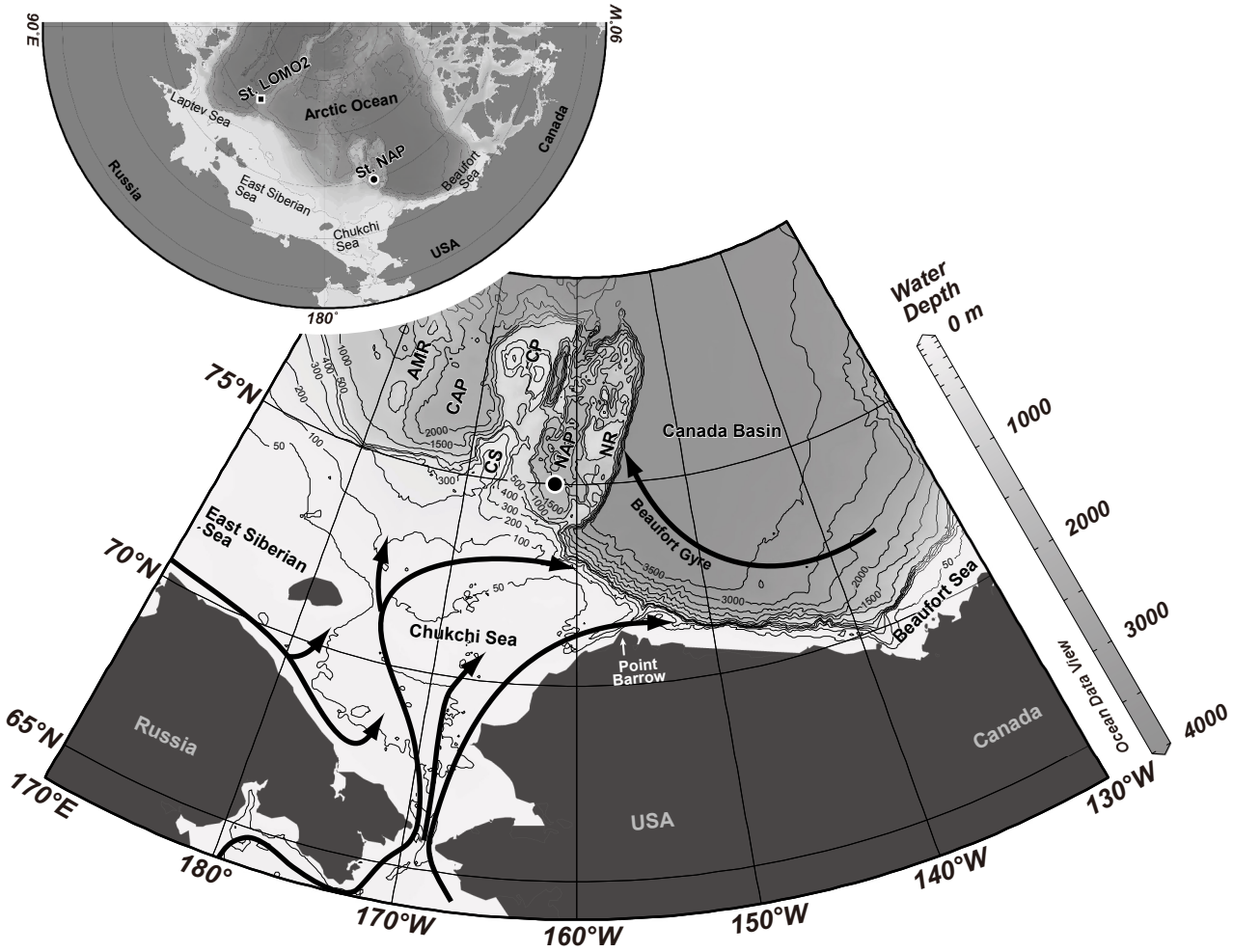
90°E
90°W
St. LOMO2
Arctic Ocean
Laptev Sea
St. NAP
Russia
East Siberian Sea
Beaufort Sea
Canada
Chukchi Sea
USA
180°
75°N
70°N
65°N
170°E
180°
170°W
160°W
150°W
140°W
130°W
AMR
CAP
CP
NAP
NR
CS
Canada Basin
Beaufort Gyre
East Siberian Sea
Chukchi Sea
Beaufort Sea
Point Barrow
Russia
USA
Canada
Water Depth
0 m
1000
2000
3000
4000
Ocean Data View

Fig. 1

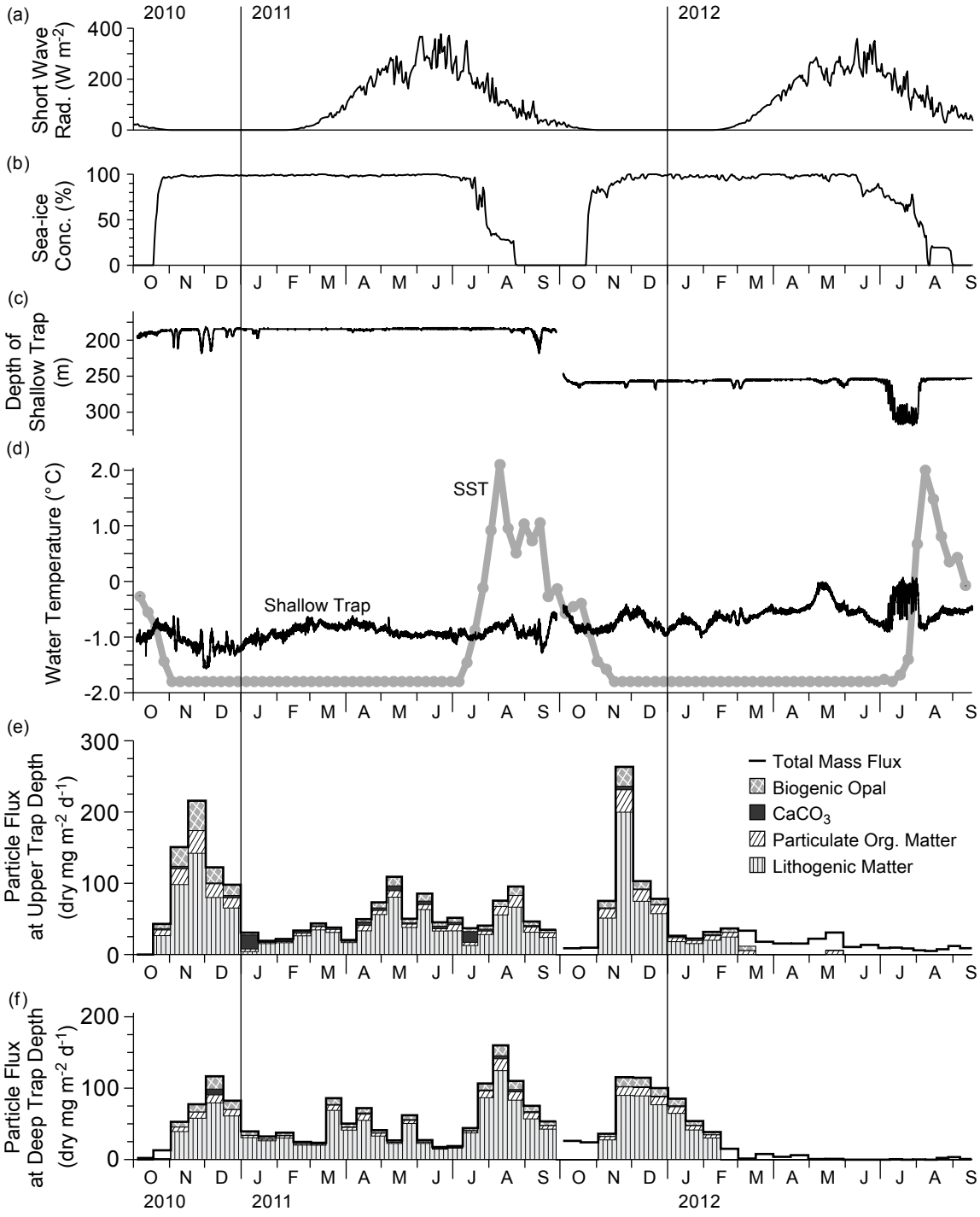
(a)
2010
2011
2012
Short Wave Rad. (W m-2)
400
200
0
(b)
Sea-ice Conc. (%)
100
50
0
O N D J F M A M J J A S O N D J F M A M J J A S
(c)
Depth of Shallow Trap (m)
200
250
300
(d)
Water Temperature (°C)
2.0
1.0
0
-1.0
-2.0
SST
Shallow Trap
(e)
Particle Flux at Upper Trap Depth (dry mg m-2 d-1)
300
200
100
0
Total Mass Flux
Biogenic Opal
CaCO3
Particulate Org. Matter
Lithogenic Matter
(f)
Particle Flux at Deep Trap Depth (dry mg m-2 d-1)
200
100
0
2010
2011
2012

Fig. 2

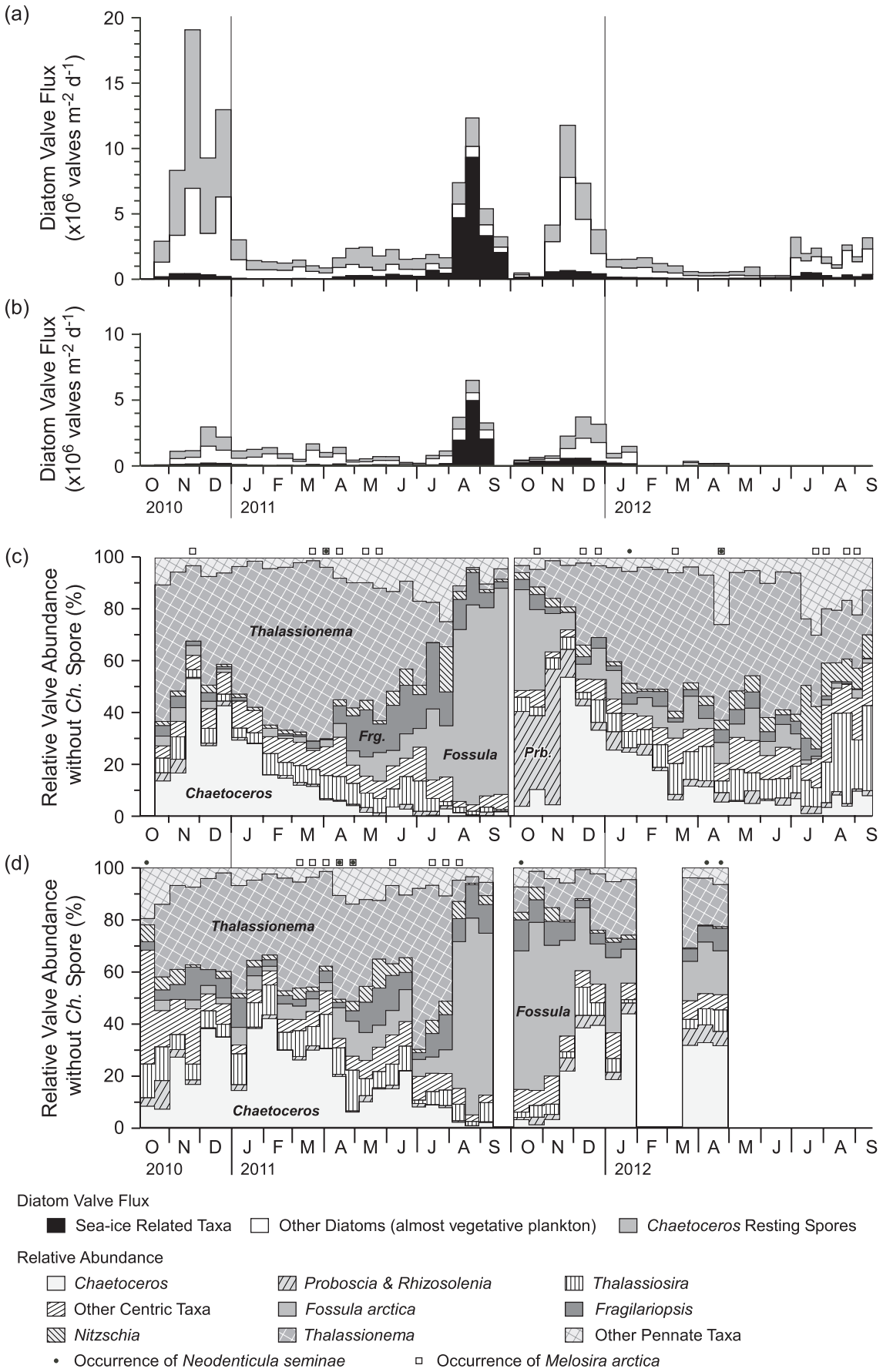
(a)
Diatom Valve Flux
(x10^6 valves m^-2 d^-1)
20
15
10
5
0
(b)
Diatom Valve Flux
(x10^6 valves m^-2 d^-1)
10
5
0
O N D J F M A M J J A S O N D J F M A M J J A S
2010
2011
2012
(c)
Relative Valve Abundance
without Ch. Spore (%)
100
80
60
40
20
0
Thalassionema
Frg.
Fossula
Prb.
Chaetoceros
O N D J F M A M J J A S O N D J F M A M J J A S
(d)
Relative Valve Abundance
without Ch. Spore (%)
100
80
60
40
20
0
Thalassionema
Fossula
Chaetoceros
O N D J F M A M J J A S O N D J F M A M J J A S
2010
2011
2012
Diatom Valve Flux
Sea-ice Related Taxa
Other Diatoms (almost vegetative plankton)
Chaetoceros Resting Spores
Relative Abundance
Chaetoceros
Proboscia & Rhizosolenia
Thalassiosira
Other Centric Taxa
Fossula arctica
Fragilariopsis
Nitzschia
Thalassionema
Other Pennate Taxa
Occurrence of Neodenticula seminae
Occurrence of Melosira arctica

Fig. 3

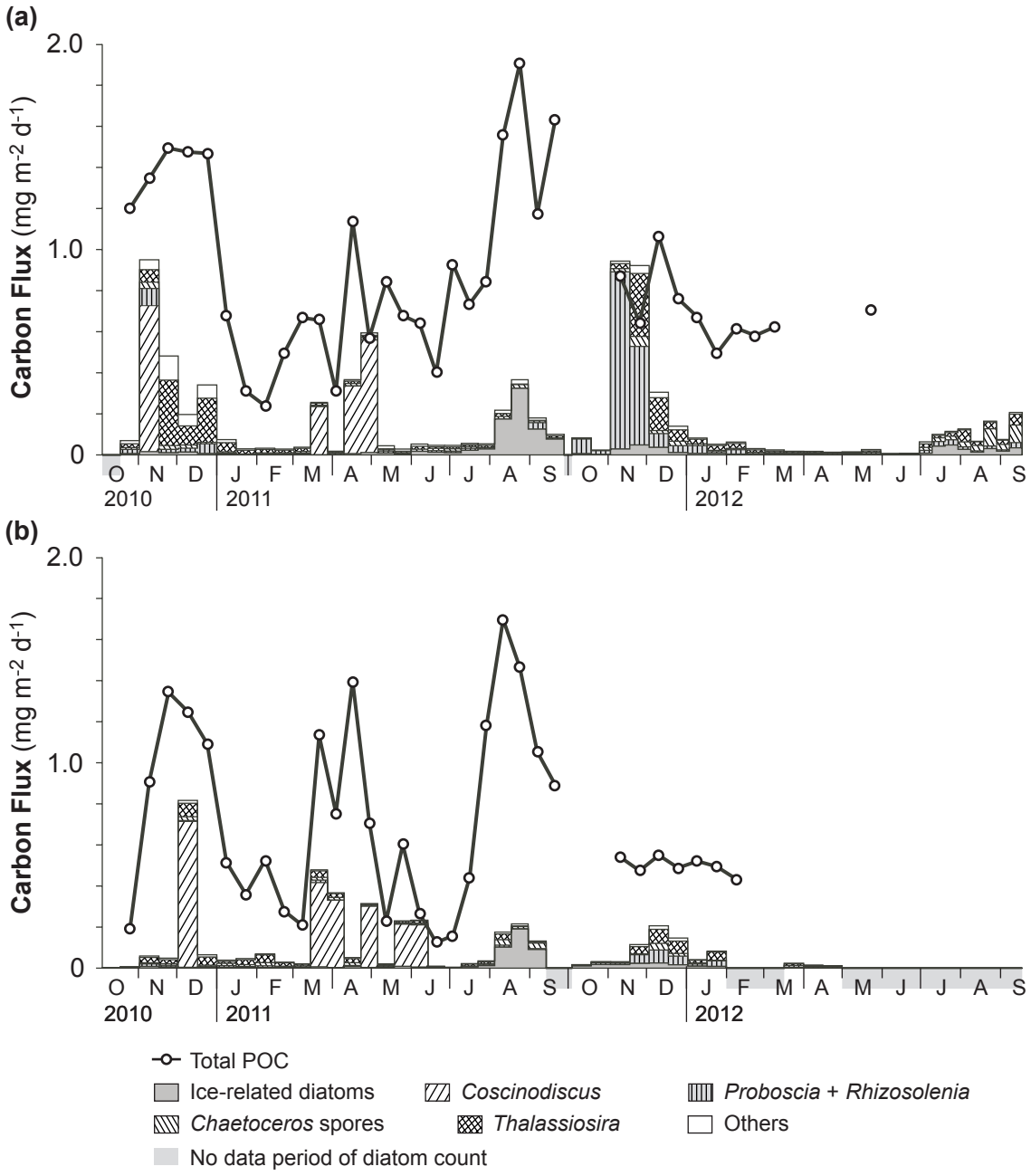
(a)
(b)
Carbon Flux (mg m-2 d-1)
2.0
1.0
0
O N D J F M A M J J A S O N D J F M A M J J A S
2010
2011
2012
Total POC
Ice-related diatoms
Coscinodiscus
Proboscia + Rhizosolenia
Chaetoceros spores
Thalassiosira
Others
No data period of diatom count

Fig. 4

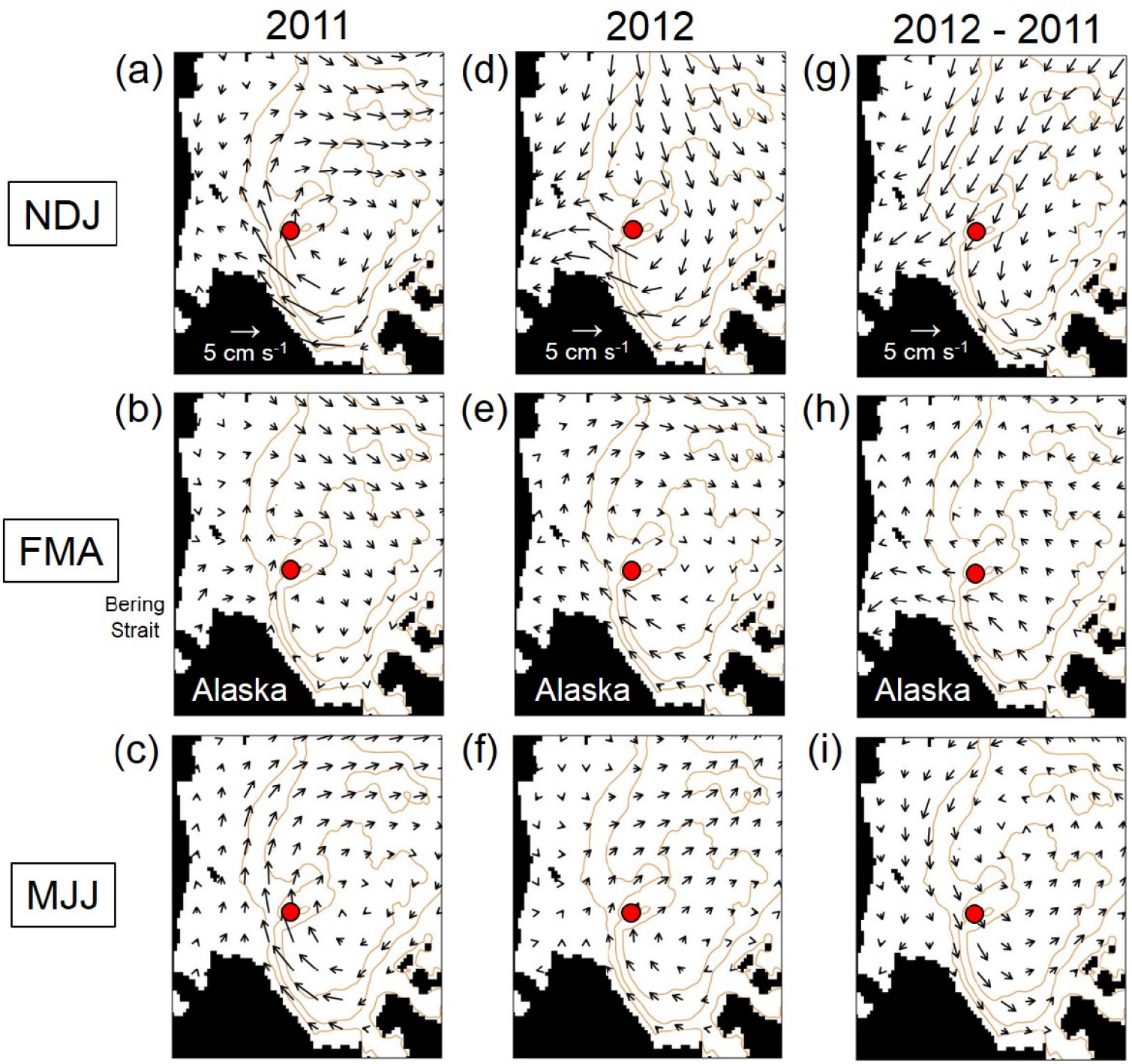
2011
2012
2012 - 2011
(a)
(d)
(g)
NDJ
5 cm s-1
5 cm s-1
5 cm s-1
(b)
(e)
(h)
FMA
Bering
Strait
Alaska
Alaska
Alaska
(c)
(f)
(i)
MJJ

Fig. 5

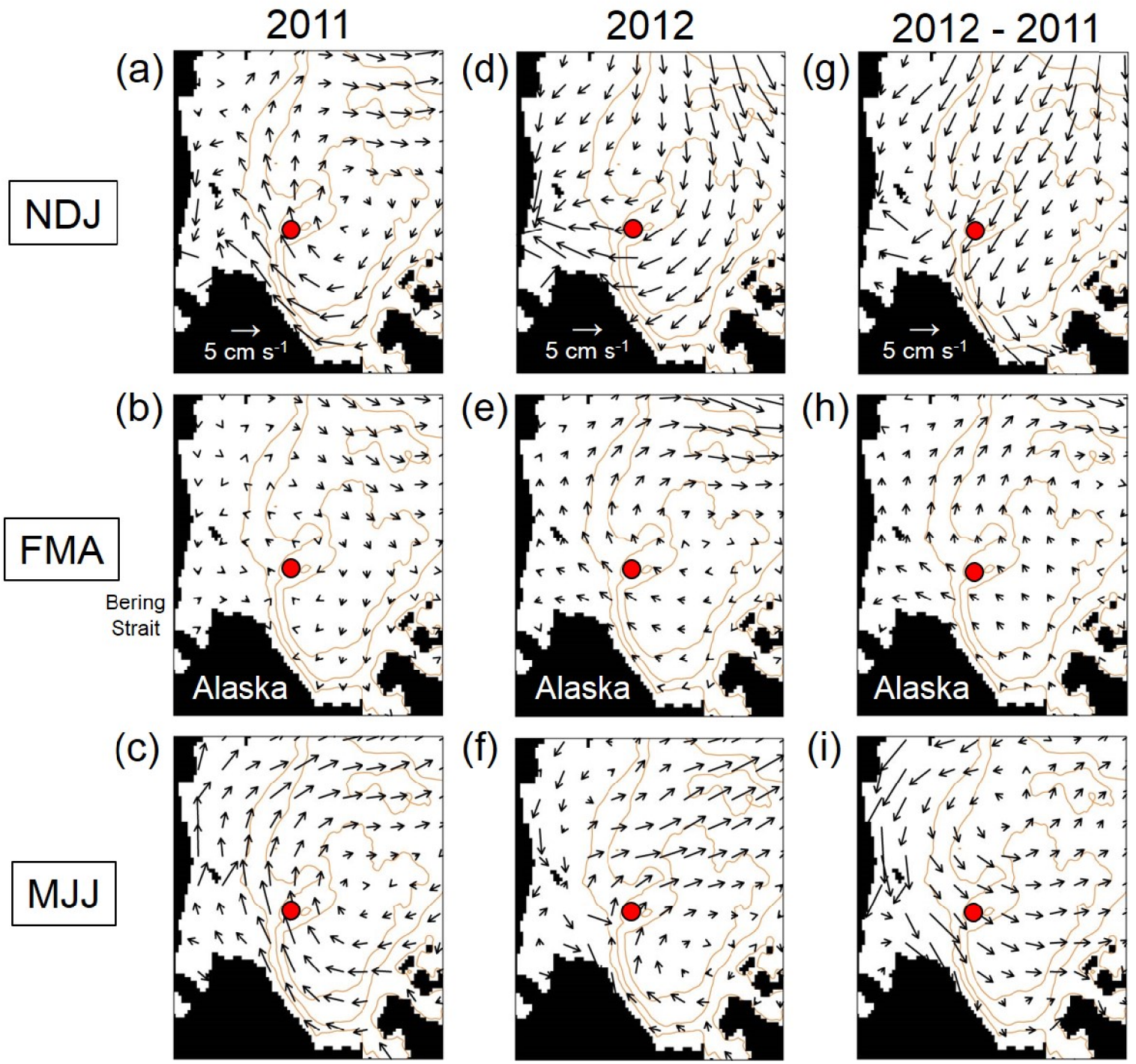
2011
2012
2012 - 2011
(a)
(b)
(c)
(d)
(e)
(f)
(g)
(h)
(i)
NDJ
FMA
MJJ
Bering Strait
Alaska
Alaska
Alaska
5 cm s-1
5 cm s-1
5 cm s-1

Fig. 6

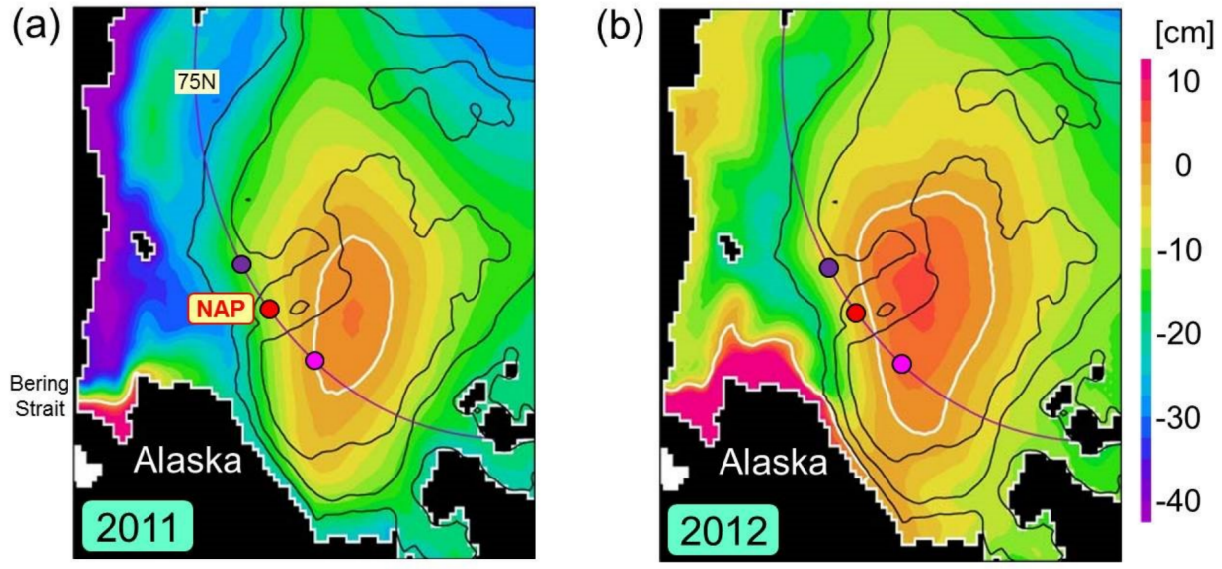
(a)
75N
NAP
Bering
Strait
Alaska
2011
(b)
Alaska
2012
[cm]
10
0
-10
-20
-30
-40

Fig. 7

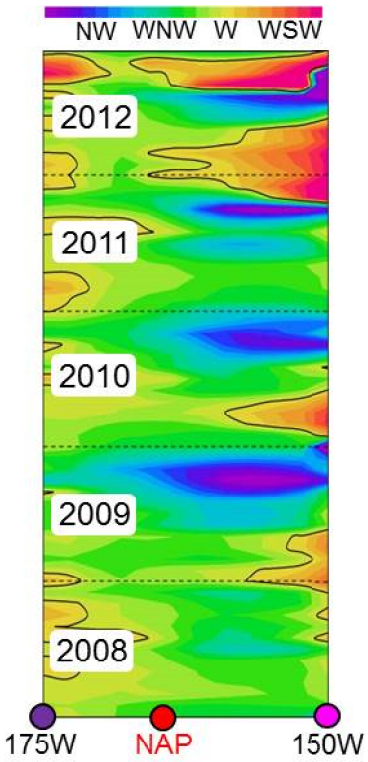

Fig. 8